# Transferred hyperfine interaction between the rare-earth ions and the fluorine nuclei in rare-earth trifluorides

**Hansen, P. E.; Nevald, Rolf; Guggenheim, H. G.**

*Published in:*
Physical Review B Condensed Matter

*Link to article, DOI:*
10.1103/PhysRevB.17.2866

*Publication date:*
1978

*Document Version*
Publisher's PDF, also known as Version of record

# Transferred hyperfine interaction between the rare-earth ions and the fluorine nuclei in rare-earth trifluorides

P. E. Hansen*, and R. Nevald
*Department of Electrophysics, The Technical University of Denmark, DK-2800 Lyngby, Denmark*
H. G. Guggenheim
*Bell Laboratories, Murray Hill, New Jersey 07974*
(Received 20 September 1977; revised manuscript received 23 November 1977)

The isotropic and anisotropic transferred hyperfine interactions between F ions in the two chemically inequivalent sites and the rare-earth ions ($R$) have been derived from $^{19}F$ NMR measurements in the temperature region 100–300 K on single crystals of $TbF_3$ and $DyF_3$. The isotropic interactions are found to be negative and constant in this temperature region and with the numerical values decreasing slightly from $TbF_3$ to $DyF_3$. The anisotropic interactions, when the point dipole contributions are subtracted, are found to be substantially smaller and about equal for the two materials. The crystals contain two symmetry related magnetic sublattices $A$ and $B$, contributing to the macroscopic susceptibility. The sublattice susceptibility has an off-diagonal component $\chi^A_{ac}$ and $\chi^B_{ac} = -\chi^A_{ac}$ in the crystalline axes system. The orientations of the principal axes of the two sublattice susceptibilities are found to vary only slightly with temperature. They are further assigned to definite $R$'s in the unit cell, which cannot be done from macroscopic magnetic measurements.

## I. INTRODUCTION

The heavy-rare-earth fluorides $RF_3$ all crystallize in the orthorhombic structure *Pnma* ($D^{12}_{2h}$) and belong to the magnetic point group *mmm*. They show a variety of interesting magnetic behavior. In that way they constitute a system well suited as testing ground for the theories of magnetic properties of rare-earth insulators. On the other hand, they have a rather complicated structure and low symmetry, which makes the interpretation of the experiments somewhat complicated.

We have undertaken an experimental study of these materials in single-crystal form from the low-temperature ordered phases to well above room temperature in the paramagnetic phases, using magnetometer and NMR techniques. Here we report the results of $^{19}F$ NMR in $TbF_3$ and $DyF_3$ between 100 and 300 K, which turns out to be a region of simple magnetic behavior compared to lower and higher temperatures. (Also the temperature region below 100 K presents a serious experimental problem, because the NMR lines become extremely broad and overlapping.)

The earliest NMR works on these materials were performed on powders,[1–5] but because of interfering resonances from two different crystalline sites, the results are of limited value. Four NMR studies have been done so far using single crystals.[6–8] Our study, however, is the first to take into consideration both the anisotropy of the macroscopic susceptibility and the nondiagonality of the sublattice susceptibility in the crystalline axes system.

## II. CRYSTALLOGRAPHIC AND MAGNETIC PROPERTIES

The *Pnma* unit cell contains four formula units of $RF_3$. The lattice constants together with other relevant parameters are collected for the two materials in Table I. For $YF_3$ it is found by Zalkin and Templeton,[9] that the four $R^{3+}$ ions are situated in the $b$ mirror planes at the (0.367, 0.25, 0.058) position and the three positions symmetry related via the $a$ and $c$ glide planes. Four of the 12 $F^-$ ions are also situated in the $b$ mirror planes at (0.528, 0.25, 0.601) and the symmetry-related positions (see Fig. 1). The other eight $F^-$ ions are at (0.165, 0.060, 0.363) and related general positions. The four and eight chemically equivalent $F^-$ ions are called $F_{(I)}$ and $F_{(II)}$, respectively. Each $F_{(I)}$ has two nearest neighbors $R$'s ~2.3 Å away and one $R$ neighbor somewhat further away ~2.6 Å. Each $F_{(II)}$ has the three nearest $R$ neighbors, which all are ~2.3 Å away. The relative positions of the ions in $TbF_3$ and $DyF_3$ are taken to be the same as in $YF_3$.

Magnetization measurements have been done for $TbF_3$ by Holmes and Guggenheim[10] and for $DyF_3$ by Johansson.[11] $TbF_3$ is found to be ferromagnetic below $T = 3.96$ K with a saturation magnetization of $8.09\mu_B$

TABLE I. Material data for $TbF_3$ and $DyF_3$ relevant for this study.

| Material | $a$ | $b$ (Å) | $c$ | $V_{cell}$ (Å$^3$) | $\kappa$ ($10^{-24}$ g) | $\rho=\frac{4\kappa}{V_{cell}}$ (g/cm$^3$) | $\frac{4}{3}\pi\rho\chi_a$ | $\frac{4}{3}\pi\rho\chi_b$ (%) | $\frac{4}{3}\pi\rho\chi_c$ |
|---|---|---|---|---|---|---|---|---|---|
| $TbF_3$ | 6.513 | 6.949 | 4.384 | 198.4 | 359 | 7.236 | 2.9 | 1.0 | 0.9 |
| $DyF_3$ | 6.460 | 6.906 | 4.376 | 195.2 | 364 | 7.456 | 2.0 | 2.5 | 1.1 |

per ion along the $a$ direction. It is further found to be possible with a magnetic field along the $c$ direction to induce a magnetization of $3.84\mu_B$ per ion along the $c$ direction. This behavior can be understood, assuming that the Tb ions are situated in two magnetically inequivalent sublattices $A$ and $B$ oriented in zero field as shown in Fig. 1(b). (This structure belongs to the magnetic space group *Pmna*.) A strong $c$ direction field induces a spin flip in one of the sublattices, so that the moment configuration becomes as shown in Fig. 1(c). (The magnetic space group changes to *Pmna*.) It is further assumed, that the Tb crystal ground level is an accidental doublet $|J=6,\ M_J=\pm 6\rangle$, having $g=\frac{3}{2}$ and therefore, $|\vec{\mu}|=9\mu_B$, so that the axis of quantization makes an angle of 25° with the $a$ direction. $DyF_3$ is found to order ferromagnetically along the $b$ direction below 2.8 K and the magnetization to be $8.4\mu_B$ per ion, where the theoretical maximum possible moment is $10\mu_B$ per ion. (The magnetic space group for this material is *Pmna*.)

In the paramagnetic phase one of the principal axes of the sublattice susceptibility tensors $\overleftrightarrow{\chi}^A$ and $\overleftrightarrow{\chi}^B$ is

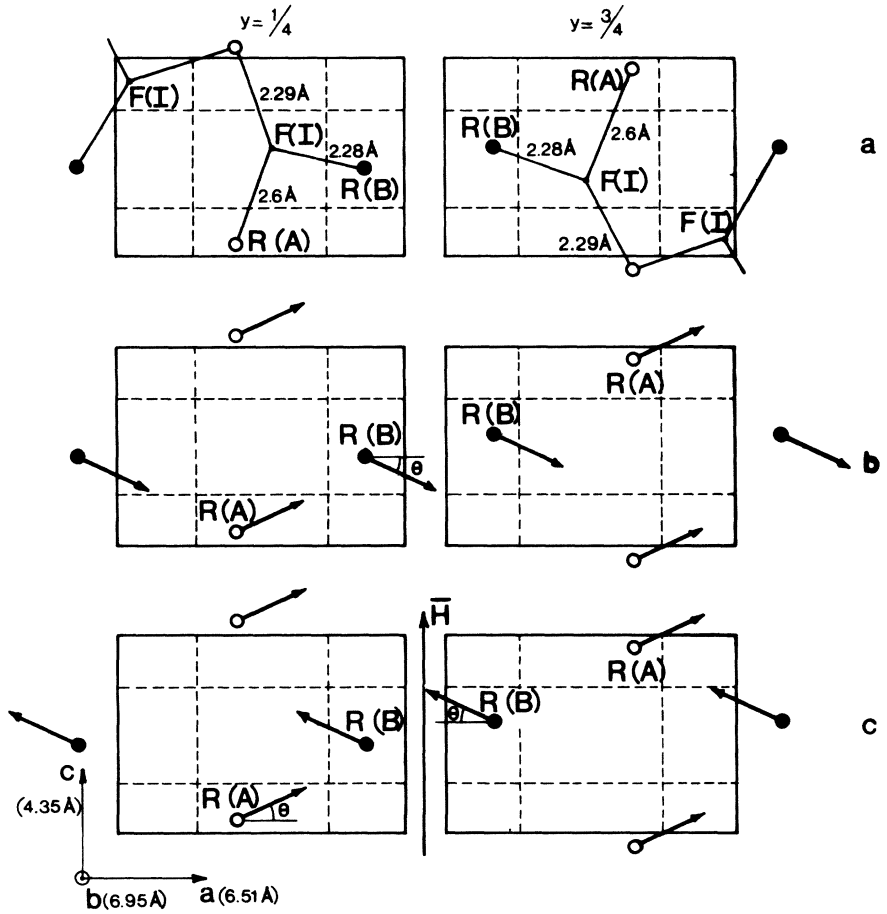


FIG. 1. (a) Arrangement of the $R$'s and the $F_{(I)}$'s in the $y=\frac{1}{4}$ and $y=\frac{3}{4}$ mirror planes for $TbF_3$ and $DyF_3$; (b) magnetic structure of $TbF_3$ in the ordered phase in zero $\vec{H}_a$ field; and (c) magnetic structure of $TbF_3$ in the ordered phase in a strong $\vec{H}_a$ field along the $c$ direction.

fixed by symmetry to be the $b$ direction, whereas the orientations of the two principal axes in the $b$ plane are not given by symmetry.

## III. THEORY

The samples used in the experiments are of spherical shape, and some of the following expressions are only valid for this case.

The effective local field at an F ion $i$ is

$$\vec{H}_i = \vec{H}_a + \vec{H}_i^{\,d} + \vec{H}_i^{\,\prime} = H_a + \sum_j \frac{[\vec{\delta}_i^{\,j} + (\zeta_i^j \vec{1} + \vec{\epsilon}_i^{\,j})]\,\vec{M}_j}{\rho}$$

$$= \vec{H}_a + \sum_j \frac{\vec{\sigma}_i^{\,j}\vec{M}_j}{\rho} \quad , \tag{1}$$

where $\vec{H}_a$ is the applied field. $\vec{H}_i^{\,d}$ and $\vec{H}_i^{\,\prime}$ are the dipole and transferred hyperfine fields from the $R$ moments. $\vec{M}_j$ is the sublattice magnetization of the $j$th sublattice ($A$ or $B$) and $\vec{\delta}_i^{\,j}$ and $\zeta_i^j\vec{1} + \vec{\epsilon}_i^{\,j}$ therefore the tensors relating the dipole and transferred hyperfine fields to the magnetizations. $\vec{\sigma}_i^{\,j} = \vec{\delta}_i^{\,j} + \zeta_i^j\vec{1} + \vec{\epsilon}_i^{\,j}$ we will call the shift tensor. The transferred hyperfine coupling is further divided into the isotropic $\zeta_i^j$ and the anisotropic traceless $\vec{\epsilon}_i^{\,j}$ part. $\rho$ is the density of the material (see Table I). (Where it is relevant, the notation is the same as introduced in Refs. 12 and 13.)

Whereas $\zeta_i^j$ and $\vec{\epsilon}_i^{\,j}$ depend in details on the electron system of the material, $\vec{\delta}_i^{\,j}$ can be calculated straightforwardly,

$$\vec{\delta}_i^{\,j} = \kappa \sum_{\substack{k \text{ in a} \\ \text{sphere}}} \frac{3\vec{r}_i^{\,(jk)}\vec{r}_i^{\,(jk)} - \vec{1}(r_i^{(jk)})^2}{(r_i^{(jk)})^5} \quad , \tag{2}$$

where $\kappa$ is the mass per formula unit and $\vec{r}_i^{\,(jk)}$ the vector from the $i$th fluorine to the $k$th $R$ ion of sublattice $j$.

At low field and far above the Curie point, which apply to the experiments presented here, the local field is

$$\vec{H}_i = \vec{H}_a + (\vec{\sigma}_i^{\,A}\chi^A + \vec{\sigma}_i^{\,B}\vec{\chi}^B)\,\vec{H}_{\text{in}}$$

$$= [\vec{1} + (\vec{\sigma}_i^{\,A}\vec{\chi}^A + \vec{\sigma}_i^{\,B}\vec{\chi}^B)$$

$$\times (\vec{1} + \tfrac{4}{3}\pi\rho\vec{\chi})^{-1}]\,\vec{H}_a \quad , \tag{3}$$

where $\vec{H}_{\text{in}}$ is the inner field, and where the sublattice susceptibilities $\vec{\chi}^A$ and $\vec{\chi}^B$ for symmetry reasons have the form

$$\vec{\chi}^A = \vec{\chi}^{\text{diag}} + \vec{\chi}^{\text{off}}, \quad \vec{\chi}^B = \vec{\chi}^{\text{diag}} - \vec{\chi}^{\text{off}},$$

$$\vec{\chi}^{\text{diag}} = \begin{pmatrix} \chi_a/2 & 0 & 0 \\ 0 & \chi_b/2 & 0 \\ 0 & 0 & \chi_c/2 \end{pmatrix},$$

$$\vec{\chi}^{\text{off}} = \begin{pmatrix} 0 & 0 & \chi_{ac} \\ 0 & 0 & 0 \\ \chi_{ac} & 0 & 0 \end{pmatrix}.$$

The maximum sizes of the small corrections

$$\tfrac{4}{3}\pi\rho\vec{\chi} = \tfrac{4}{3}\pi\rho 2\,\vec{\chi}^{\text{diag}} \tag{4}$$

are found in Table I.

In the crystalline and in the sublattice susceptibility principle coordinate systems, respectively, $\vec{\chi}^A$ has the form

$$\vec{\chi}^A = \begin{pmatrix} \chi_a/2 & 0 & \chi_{ac} \\ 0 & \chi_b/2 & 0 \\ \chi_{ac} & 0 & \chi_c/2 \end{pmatrix}$$

and

$$\vec{\chi}^A = \begin{pmatrix} \chi_x & 0 & 0 \\ 0 & \chi_b/2 & 0 \\ 0 & 0 & \chi \end{pmatrix} \quad , \tag{5}$$

where

$$\chi_{xz} = 0 = \chi_{ac}\cos 2\theta + \tfrac{1}{2}(\chi_c - \chi_a)\sin 2\theta$$

or

$$\theta(T) = \tfrac{1}{2}\arctan\frac{2\chi_{ac}(T)}{\chi_a(T) - \chi_c(T)} \quad ,$$

with $\theta$ being the angle between the $a$ and $x$ axis.

In NMR the relative line shifts $K_i$ are measured, which using Eqs. (3) become

$$K_i = (H_i - H_a)/H_a = \vec{1}_H(\vec{\sigma}_i^{\,+}\vec{\chi}^{\text{diag}} + \vec{\sigma}_i^{\,-}\vec{\chi}^{\text{off}})$$

$$\times (\vec{1} + \tfrac{4}{3}\pi\rho\vec{\chi})^{-1}\vec{1}_H \quad ,$$

$$\vec{\sigma}_i^{\,\pm} = \vec{\sigma}_i^{\,A} \pm \vec{\sigma}_i^{\,B} \quad , \tag{6}$$

with $\vec{1}_H$ being a unit vector along $\vec{H}_a$. [Although the corrections $(\vec{1} + \frac{4}{3}\pi\rho\vec{\chi})^{-1}$ have been used in the analysis of the data they will be omitted in the following formulas for clarity.]

There are 12 $\vec{\sigma}_i^{\,\pm}$ to consider with $i$ running over the 12 F ions in the unit cell. Because the four F(I)'s are situated in the $b$ mirror planes, the corresponding $\vec{\sigma}_i^{\,\pm}$ have the form

$$\vec{\sigma}_1^{\,\pm} \equiv \vec{\sigma}_{11}^{\,\pm} = \vec{\sigma}_{13}^{\,\pm} = \begin{pmatrix} \sigma_{1aa}^{\pm} & 0 & \sigma_{1ac}^{\pm} \\ 0 & \sigma_{1bb}^{\pm} & 0 \\ \sigma_{1ac}^{\pm} & 0 & \sigma_{1cc}^{\pm} \end{pmatrix}$$

and

$$\vec{\sigma}_{12}^{\,\pm} = \vec{\sigma}_{14}^{\,\pm} = \begin{pmatrix} \pm\sigma_{1aa}^{\pm} & 0 & \mp\sigma_{1ac}^{\pm} \\ 0 & \pm\sigma_{1bb}^{\pm} & 0 \\ \mp\sigma_{1ac}^{\pm} & 0 & \pm\sigma_{1cc}^{\pm} \end{pmatrix} \quad , \tag{7}$$

with those $F_{(I)}$ related through the inversion centers of the structure having $\vec{\sigma}_i^{\,\pm}$ equal.

For the eight $F_{(II)}$, being in general positions, all tensor components are nonzero. Also $F_{(II)}$ related via the inversion centers have $\vec{\sigma}_i^{\pm}$ equal:

$$\vec{\sigma}_{II}^{\pm} \equiv \vec{\sigma}_{III}^{\pm} = \vec{\sigma}_{II5}^{\pm} = \begin{pmatrix} \sigma_{II\bar{a}a}^{\pm} & \sigma_{II\bar{a}b}^{\pm} & \sigma_{II\bar{a}c}^{\pm} \\ \sigma_{II\bar{a}b}^{\pm} & \sigma_{II\bar{b}b}^{\pm} & \sigma_{II\bar{b}c}^{\pm} \\ \sigma_{II\bar{a}c}^{\pm} & \sigma_{II\bar{b}c}^{\pm} & \sigma_{II\bar{c}c}^{\pm} \end{pmatrix} ,$$

$$\vec{\sigma}_{II2}^{\pm} = \vec{\sigma}_{II6}^{\pm} = \begin{pmatrix} + & - & + \\ - & + & - \\ + & - & + \end{pmatrix} ,$$

$$\vec{\sigma}_{II3}^{\pm} = \vec{\sigma}_{II7}^{\pm} = \begin{pmatrix} \pm & \mp & \mp \\ \mp & \pm & \pm \\ \mp & \pm & \pm \end{pmatrix} , \qquad (8)$$

and

$$\vec{\sigma}_{II4}^{\pm} = \vec{\sigma}_{II8}^{\pm} = \begin{pmatrix} \pm & \pm & \mp \\ \pm & \pm & \mp \\ \mp & \mp & \pm \end{pmatrix} ,$$

where for brevity only the sign of the components, for the tensors symmetry related to $\vec{\sigma}_{III}$ and $\vec{\sigma}_{II5}$, are shown, because the numerical values are the same for all eight tensors. [Note—what at first might be a surprise—that the sign of the $ac$ components of $\vec{\sigma}_i^{-}$ is the same for all four $F_{(I)}$ and for all eight $F_{(II)}$.]

As can be seen from Eqs. (6)–(8), the $F_{(I)}$ and $F_{(II)}$ give rise to two and four NMR lines, respectively, when the field is applied in a general direction. For the field limited to rotations in the crystalline planes, the Fourier components of the shifts are evaluated from Eq. (6) and presented in Table II. The two $F_{(I)}$ NMR lines coalesce into one in the $a$ and $c$ planes, and the four $F_{(II)}$ lines into two in all three planes for symmetry reasons. Furthermore with the field along any of the crystalline axes $F_{(I)}$ and $F_{(II)}$ give rise to only one line each. Figure 2 shows the experimental $TbF_3$ NMR rotation pattern at 300 K for $\vec{H}_a$ rotating $a \rightarrow b \rightarrow c \rightarrow a$. One notes that it agrees with the stated symmetry requirements.

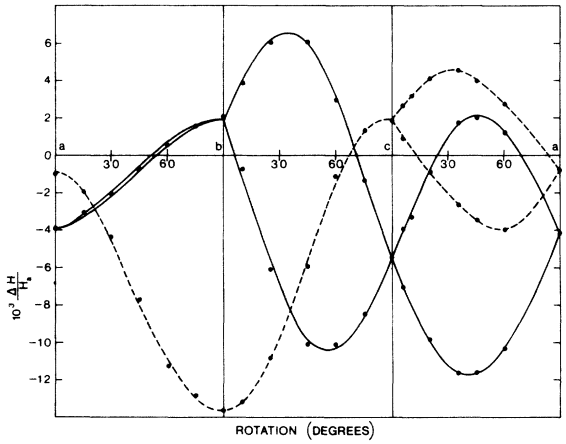


FIG. 2. Experimental NMR rotation pattern for $\vec{H}_a$ rotating $a \rightarrow b \rightarrow c \rightarrow a$ at 300 K for $TbF_3$. Solid lines, $F_{(II)}$ resonances; dashed lines, $F_{(I)}$ resonances.

In principle the maximum amount of experimental information is available from these rotation spectra taken at various temperatures. In practice, however, it turns out that the NMR linewidth inhibits sufficient accuracy in the experimental values of the product of the appropriate susceptibility component and $\sigma_{i\bar{a}a}^{-}$, $\sigma_{i\bar{c}c}^{-}$, $\sigma_{II\bar{a}b}^{-}$, $\sigma_{II\bar{b}c}^{-}$, $\sigma_{II\bar{a}c}^{+}$ or one of the three off-diagonal components of $\vec{\sigma}_{II}^{+}$. Therefore, we limit the discussion to $\sigma_{I\bar{a}c}^{-}$, $\sigma_{II\bar{a}c}^{-}$, and the diagonal components of $\vec{\sigma}_{I}^{+}$ and $\vec{\sigma}_{II}^{+}$. These eight quantities, as we shall see, give interesting and convincing evidence for a simple $\vec{\sigma}_i^{\pm}$ behavior.

One should note from Table II, that this limited number of $\vec{\sigma}_i^{\pm}$ components can be derived solely from the shift measurements with $\vec{H}_a$ along the crystalline

TABLE II. Fourier components of the NMR rotation spectra, for rotating in the three crystalline planes $a \rightarrow b$, $b \rightarrow c$, $c \rightarrow a$, in the expression

$$\frac{\Delta H_i(\phi)}{H_a} = K_i^{\cos}\cos^2\phi + K_i^{cs}\cos\phi\sin\phi + K_i^{\sin}\sin^2\phi ,$$

$K_I^{cs} = 0$ for $a \rightarrow b$ and $b \rightarrow c$. (Note that $K_i^{\cos}$ is also the shift $K_i^{\alpha}$ for $\vec{H}_a$ applied along the starting crystalline axis $\alpha$ of the rotation spectrum.)

| $H_a$ rotation | $K_i^{\cos}$ | $K_i^{cs}$ | $K_i^{\sin}$ |
|---|---|---|---|
| $a \rightarrow b$ | $\sigma_{i\bar{a}a}^{+}\chi_a + \sigma_{i\bar{a}c}^{-}\chi_{ac}$ | $\pm[\sigma_{i\bar{a}b}^{+}(\chi_a + \chi_b) + \sigma_{i\bar{b}c}^{-}\chi_{ac}]$ or 0 | $\sigma_{i\bar{b}b}^{+}\chi_b$ |
| $b \rightarrow c$ | $\sigma_{i\bar{b}b}^{+}\chi_b$ | $\pm[\sigma_{i\bar{b}c}^{+}(\chi_b + \chi_c) + \sigma_{i\bar{a}b}^{-}\chi_{ac}]$ or 0 | $\sigma_{i\bar{c}c}^{+}\chi_c + \sigma_{i\bar{a}c}^{-}\chi_{ac}$ |
| $c \rightarrow a$ | $\sigma_{i\bar{c}c}^{+}\chi_c + \sigma_{i\bar{a}c}^{-}\chi_{ac}$ | $\pm[\sigma_{i\bar{a}c}^{+}(\chi_c + \chi_a) + (\sigma_{i\bar{a}a}^{-} + \sigma_{i\bar{c}c}^{-})\chi_{ac}]$ | $\sigma_{i\bar{a}a}^{+}\chi_a + \sigma_{i\bar{a}c}^{-}\chi_{ac}$ |

TABLE III. Dipole tensors $\overleftrightarrow{\delta}_I^{\pm}$ and $\overleftrightarrow{\delta}_{II}^{\pm}$ and their fastest variance with $F_I$ and $F_{II}$ translations $|\nabla_{\vec{r}_F}\overleftrightarrow{\delta}_i^{\pm}(\vec{r}_F)|$ for $TbF_3$ and $DyF_3$, calculated by lattice summation over spheres with radius 25 Å and checking for convergence (estimated uncertainty of F positions is $\pm 3\times10^{-2}$ Å on all coordinates not fixed by symmetry, giving a systematic uncertainty on the $\overleftrightarrow{\delta}_i^{\pm}$ components of interest to us of the order of $\pm 4$ g/cm$^3$ for both sites).

| Material | site | Sublattice sum (+) or difference (−) | $\overleftrightarrow{\delta}_i^{\pm}$(g/cm$^3$) | | | | | | $\lvert\nabla_{\vec{r}_F}\overleftrightarrow{\delta}_i^{\pm}(\vec{r}_F)\rvert$ (g/cm$^3$/10$^{-2}$ Å) | | | | | |
|---|---|---|---|---|---|---|---|---|---|---|---|---|---|---|
| | | | *a* | *b* | *c* | *bc* | *ca* | *ab* | *a* | *b* | *c* | *bc* | *ca* | *ab* |
| $TbF_3$ | I | + | 22 | −63 | 41 | 0 | 35 | 0 | 1.1 | 0.3 | 1.3 | ··· | 4.5 | ··· |
| | | − | −91 | −1 | 93 | 0 | −5 | 0 | 0.9 | 0.7 | 1.5 | ··· | 0.9 | ··· |
| | II | + | −3 | 34 | −31 | −41 | 33 | −1 | 0.9 | 1.0 | 0.4 | 1.6 | 0.5 | 1.0 |
| | | − | 10 | −48 | 38 | −4 | 13 | −56 | 0.9 | 0.9 | 0.8 | 0.8 | 0.4 | 0.8 |
| $DyF_3$ | I | + | 24 | −67 | 43 | 0 | 38 | 0 | 1.1 | 0.3 | 1.3 | ··· | 4.5 | ··· |
| | | − | −99 | −1 | 100 | 0 | −6 | 0 | 0.9 | 0.7 | 1.5 | ··· | 0.9 | ··· |
| | II | + | −3 | 37 | −33 | −42 | 36 | −1 | 0.9 | 1.0 | 0.4 | 1.6 | 0.5 | 1.0 |
| | | − | 10 | −52 | 42 | −3 | 14 | −61 | 0.9 | 0.9 | 0.8 | 0.8 | 0.4 | 0.8 |

*a*, *b*, and *c* axes. Therefore, only the temperature dependence of these shifts (called $K'_\alpha$ for $\vec{H}_a\|\vec{\alpha}$, $i=$ I or II, $\alpha=a$, *b*, or *c*) will be studied in detail.

Whereas the temperature dependence of $\overleftrightarrow{\delta}_i^{\pm}$ probably is negligible, being of the order of the temperature dependence of the crystalline volume, all other quantities may in general be essentially temperature dependent:

$$\left.\begin{aligned} K'_\alpha(T) &= \sigma^{+}_{i\alpha\alpha}\chi_\alpha + \sigma^{-}_{iac}\chi_{ac} \\ &= [\delta^{+}_{i\alpha\alpha} + \zeta_i^{+}(T) + \epsilon^{+}_{i\alpha\alpha}(T)]\chi_\alpha(T) \\ &\quad + [\delta^{-}_{iac} + \epsilon^{-}_{iac}(T)]\chi_{ac}(T)\ , \\ \alpha &= a \text{ or } c \\ K'_b(T) &= \sigma^{+}_{ibb}\chi_b \\ &= [\delta^{+}_{ibb} + \zeta_i^{+}(T) + \epsilon^{+}_{ibb}(T)]\chi_b(T) \end{aligned}\right\} i=\text{I, II}\ . \quad (9)$$

A problem in trying to determine the transferred hyperfine quantities from Eq. (9) is, that $\chi_{ac}(T)$ cannot be found from macroscopic measurements, because the two sublattice contributions cancel out.

Eliminating the terms containing $\chi_{ac}(T)$, leave two experimental quantities per F site, the temperature behavior of which is to be considered:

$$K'_{ac}(T) \equiv K'_a(T) - K'_c(T) \quad (10a)$$

$$= \sigma^{+}_{iaa}(T)\chi_a(T) - \sigma^{+}_{icc}(T)\chi_c(T)$$

$$K'_b(T) = \sigma^{+}_{ibb}(T)\chi_b(T) \quad (10b)$$

$i=$ I, II .

From the known crystal structure the four dipole tensors $\overleftrightarrow{\delta}_i^{\pm}$ ($i=$ I and II) for $TbF_3$ and $DyF_3$ are calculated using Eq. (2) and summing over spheres with radius 25 Å and checking for convergence. The results are shown in Table III, and because the F positions are somewhat uncertain $|\nabla_{\vec{r}_F}\overleftrightarrow{\delta}_i(r_F)|$ (in g/cm$^3$/10$^{-2}$ Å) are also included. [$|\nabla_{\vec{r}_F}\overleftrightarrow{\delta}_i(r_F)|$ is the fastest variance of $\overleftrightarrow{\delta}_i(\vec{r}_F)$ for F translations.]

## IV. EXPERIMENTAL PROCEDURE

The single crystals of $TbF_3$ and $DyF_3$, grown from the melt using a modified Stockbarger technique,[14] were ground into spheres of approximately 2-mm diameter with a sphericality better than 1%. The spheres were oriented by conventional Laue x-ray technique, and the orientations were checked directly in the NMR sample holder.

Some NMR rotation spectra were taken to check the overall behavior at room temperature, at liquid-$N_2$ temperature and at an intermediate temperature, but most NMR measurements were performed with the $\vec{H}_a$ field along either the *a*, *b*, or *c* axis of the crystal. In these measurements the deviation between the $\vec{H}_a$ direction and the crystalline axis was always less than one degree.

As shown in Fig. 3 a self-supporting five-turn coil of lacquered copper wire 0.4 mm in diameter was placed around the sample and connected through a 0.5-m-long silvered coaxial line to a Robinson-type NMR spectrometer. The spectrometer frequency was kept fixed around 32 MHz and the magnetic field swept through the resonances and monitored with a field-locked NMR gaussmeter.

The temperature was monitored and regulated by means of a four point measurement of the resistance of a copper wire, 1 m long and 0.03 mm in diameter, induction free wound in close proximity to the sample. The sample compartment was evacuated and submerged in liquid nitrogen, and the sample was heated by a copper wire 0.07 mm in diameter induction free wound on a brass tube surrounding the sample. The temperature was kept fixed to within 0.2 K during an NMR scan, which lasted ~15 min. [The Ge thermometer is for low-temperature measurements and not used in the experiments described here.]

## V. RESULTS

The measured $K'_\alpha(R)$'s are shown in Fig. 4(a) for $TbF_3$ and in 4(b) for $DyF_3$. The NMR linewidth versus temperature is indicated, and it can be seen that especially for $TbF_3$, the accuracy of the experimentally determined shifts will deteriorate fast below 100 K. The macroscopic susceptibilities $\overleftrightarrow{\chi}$ are also included in Fig. 4(c) and 4(d) for comparison. It can be seen that $K'_b(T)$ and $\chi_b(T)$ are proportional, whereas $K'_\alpha(T)$ and $\chi_\alpha(T)$ for $\alpha = a$ or $c$ are not. The proportionality between $K'_b(T)$ and $\chi_b(T)$ means that $\sigma^+_{ibb}$ is, in fact, independent of temperature in the temperature region considered.

In the following procedure for extracting the transferred hyperfine parameters, average experimental shifts and macroscopic susceptibilities at six representative temperatures $T_n = 105$, 120, 145, 175, 220, and 300 K, are used.

In Table IV, $\sigma^+_{ibb}$ for the two materials, and the experimental standard deviation

$$S'_b = \left\{ \frac{1}{5} \sum_{n=1}^{6} [K'_b(T_n) - \sigma^+_{ibb}\chi_b(T_n)]^2 \right\}^{1/2} , \quad i = \mathrm{I}, \mathrm{II} \tag{11}$$

is first shown. $\sigma^+_{\mathrm{I}bb}$ for $DyF_3$—derived from by far the largest experimental shift, $K^b_{\mathrm{I}}$ (105 K) $\simeq -67 \times 10^{-3}$—might show a slight increase with temperature of ~1.5% going from 300 to 105 K. But apart from that case, $\sigma^+_{ibb}$ stays constant, considering the experimental inaccuracy of the measured shifts of $\sim \pm 0.3 \times 10^{-3}$.

$\sigma^+_{ibb}$ in general being temperature independent inside the experimental accuracy, suggests that also $\sigma^+_{iaa}$ and $\sigma^+_{icc}$ might be temperature independent. Therefore it is next examined, whether Eq. (10a) is well satisfied for some set $(\sigma^+_{iaa}, \sigma^+_{icc})$. Such a set turns out to exist in all four cases. The corresponding minimum in the standard deviation

$$S'_{ac} = \left\{ \frac{1}{5} \sum_{n=1}^{6} [K'_{ac}(T_n) - \sigma^+_{iaa}\chi_a(T_n) - \sigma^+_{icc}\chi_c(T_n)]^2 \right\}^{1/2} \tag{12}$$

lies inside the experimental accuracy. $\sigma^+_{iaa}$, $\sigma^+_{icc}$, and $S'_{ac}$ are included in Table IV.

Further

$$\zeta_i^+ = \tfrac{1}{3}(\sigma_{iaa} + \sigma_{ibb} + \sigma_{icc}) \ , \quad \delta^+_{i\alpha\alpha} + \epsilon^+_{i\alpha\alpha} = \sigma^+_{i\alpha\alpha} - \zeta_i^+ \ ,$$

and (using the calculated $\delta^+_{i\alpha\alpha}$) $\epsilon^+_{i\alpha\alpha}$ with $\alpha = a$, $b$, and $c$ are extracted and presented in Table IV.

Finally, knowing $(\sigma^+_{iaa}, \sigma^+_{icc})$, $\sigma^-_{iac}(T_n)\chi_{ac}(T_n)$ are derived from Eq. (9) and compiled in Table V. As an example the contributions $\chi_\alpha \sigma^+_{i\alpha\alpha}$ and $\chi_{ac}\sigma^-_{iac}$ to $K'_\alpha$ ($\alpha = a$ or $c$) is shown for $TbF_3$ in Fig. 5. Also presented in Table V is

$$\tfrac{1}{2}\sigma^-_{iac}(T_n)\tan 2\theta(T_n) = \frac{\sigma^-_{iac}(T_n)\chi_{ac}(T_n)}{\chi_c(T_n) - \chi_a(T_n)} \ .$$

For site-II F this quantity is experimentally undetermined at temperatures above ~175 K due to its smallness. For site-I F and for site-II F at lower temperatures it is seen to depend much less on temperature than $\chi$. It might well be that $\sigma^-_{iac}$ is temperature independent and only $\theta(T_n)$ is changing some (~5) degrees in the temperature region considered.

TABLE IV. The diagonal components of the tensors $\overleftrightarrow{\sigma}_i^+$, $(\overleftrightarrow{\delta}_i^+ + \overleftrightarrow{\epsilon}_i^+)$, and $\overleftrightarrow{\epsilon}_i^+$ and the isotropic transferred hyperfine coupling $\zeta_i$ (in g/cm$^3$). For comparison $\frac{4}{3}\pi\rho$ is ~30 g/cm$^3$. The standard deviation between measured shifts $K_i^\alpha$ and the best fitting shift tensor diagonal components (in units of $10^{-3}$). Accuracy of the measured shifts $\sim \pm 0.3 \times 10^{-3}$. (The diagonal components of $\epsilon_i^+$ are not very well determined, due to the experimental inaccuracy of ±1 g/cm$^3$ and the systematic uncertainty of ±4 g/cm$^3$ coming from F-position uncertainties.)

| Material | Site $i$ | $\sigma^+_{ibb}$ | $S'_b$ | $\sigma^+_{iaa}$ | $\sigma^+_{icc}$ | $S'_{ac}$ | $\zeta_i^+$ | $\delta^+_{iaa}+\epsilon^+_{iaa}$ | $\delta^+_{ibb}+\epsilon^+_{ibb}$ | $\delta^+_{icc}+\epsilon^+_{icc}$ | $\epsilon^+_{iaa}$ | $\epsilon^+_{ibb}$ | $\epsilon^+_{icc}$ |
|---|---|---|---|---|---|---|---|---|---|---|---|---|---|
| $TbF_3$ | I | −75.9 | 0.2 | 2.7 | 31.8 | 0.2 | −13.8 | 16.5 | −62.1 | 45.6 | −5 | 1 | 4 |
| | II | 9.4 | 0.1 | −17.5 | −40.6 | 0.1 | −16.2 | −1.3 | 25.6 | −24.4 | 2 | −8 | 6 |
| $DyF_3$ | I | −77.6 | 0.4 | 4.1 | 34.8 | 0.3 | −12.9 | 17.0 | −64.7 | 47.7 | −7 | 2 | 5 |
| | II | 18.2 | 0.2 | −15.0 | −43.2 | 0.1 | −13.3 | −1.7 | 31.5 | −29.9 | 1 | −5 | 3 |
| Accuracy | | ±1 | ··· | ±1 | ±1 | ··· | ±1 | ±1 | ±1 | ±1 | ±1 + (systematic ±4) | | |

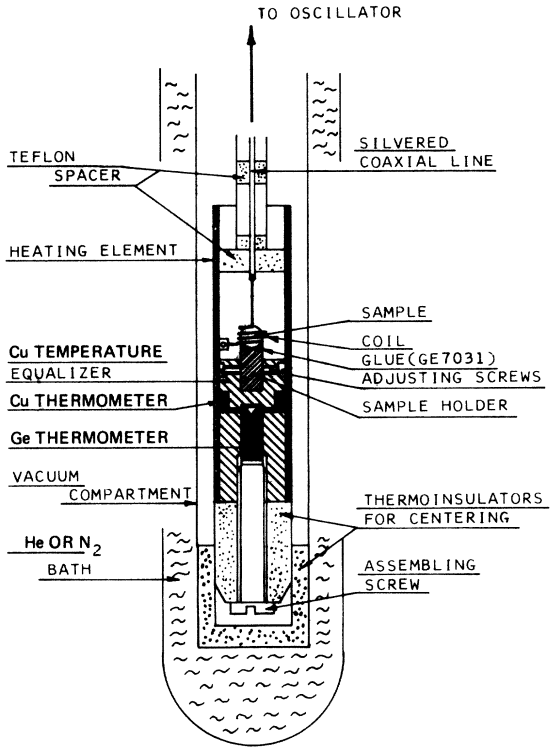


FIG. 3. Setup for NMR measurements on spherical (magnetic) samples at various temperatures.

## VI. DISCUSSION

In recent years considerable doubt has been raised to the viewpoint that isotropic and anisotropic hyperfine coupling strengths are essentially temperature independent. Some experimental evidence exists, which indicates that an appreciable change of strength may occur between room temperatures and liquid-He temperatures.[15] Also it has been calculated, using the covalent model of spin transfer,[16] that such a change is theoretically possible, originating in the very different population of the crystal split-ground multiplet in the two temperature regions. The present paper shows that from 100 to 300 K the isotropic strength $\zeta_i^+$ does not change appreciably with temperature. Whether any change would appear, if linewidth had allowed data to be taken at still lower temperatures, is of course not known. However, in studies of somewhat similar systems, where we have been able to follow the NMR lines all the way down to liquid-He temperatures, no strong change in the coupling strengths has been found.[17]

The isotropic transferred hyperfine couplings $\zeta_i^+$ are negative and of the same order of magnitude for both F sites and both materials. (That they are negative means by our convention that the effective field is smaller than it would have been without the coupling.) This is similar to what we have found for the $LiRF_4$ system.[13] The accuracy of $\sim\pm1$ g/cm$^3$ does not call for a detailed comparison between the various $\zeta_i^+$. Two features, however, should be noted: (i) the numerical values for $TbF_3$ are somewhat larger than for $DyF_3$ and this seems to be a trend also found for other groups of materials containing Tb or Dy; (ii) while $F_{(II)}$ has three $R$ neighbors all $\sim2.3$ Å away, only two of the three $R$ neighbors of $F_{(I)}$ is 2.3 Å away and the third $\sim2.6$ Å away. Thus it is reasonable that the absolute value of $\zeta_{II}^+$ is larger than that of $\zeta_I^+$. A similar relation is found between $\zeta_{II}^+$ and $\zeta_I^+$ in $ErF_3$ by Mustafa *et al.*[8]

As mentioned earlier, the uncertainty in the correct F positions ($\sim\pm3\times10^{-2}$ Å on coordinates not fixed by symmetry), caused the calculated dipole tensor components $\delta_{i\alpha\alpha}^+$ to have systematic uncertainties, which we judge to be $\sim\pm4$ g/cm$^3$. This means that the anisotropic transferred hyperfine tensor components $\epsilon_{i\alpha\alpha}^+$ are not well determined. It can, however, be stated that it is not possible with any reasonable set of $\delta_{i\alpha\alpha}^+$ values to bring all $\epsilon_{i\alpha\alpha}^+$ near to zero. We therefore conclude that $\bar{\epsilon}_i^+$ is not vanishingly small, but appreciably smaller than $\zeta_i^+$. It should also be pointed out that for a given F site, the $\epsilon_{i\alpha\alpha}^+$ values are not entirely uncorrelated comparing the two materials. This observation gives further confidence in the reality of nonvanishing $\bar{\epsilon}_i^+$'s.

Also the smallness of the anisotropic transferred hyperfine interaction, compared to the isotropic one, seems to be a universal feature, when rare-earth ions are involved, as can be seen from a comparison to Refs. 8 and 13.

In Table V the values of $\sigma_{i\bar{a}c}\chi_{ac}$ and of

$$\tfrac{1}{2}\sigma_{i\bar{a}c}\tan2\theta=\sigma_{i\bar{a}c}\chi_{ac}/(\chi_a-\chi_c)$$

are collected. Also included as an aid in the discussion is $\delta_{i\bar{a}c}$ and its uncertainty $\pm\Delta\delta_{i\bar{a}c}$. First it is seen that the two materials show large similarities in these parameters, and therefore they will be discussed together. On the one hand, it is noted that $\sigma_{I\bar{a}c}\chi_{ac}$ and $\sigma_{II\bar{a}c}\chi_{ac}$ have opposite sign, corresponding to what has been calculated for $\delta_{I\bar{a}c}$ and $\delta_{II\bar{a}c}$. On the other hand, while the ratio $\sigma_{I\bar{a}c}/\sigma_{II\bar{a}c}$ only can vary between $-3.5$ and $-6.5$ due to the experimental inaccuracy, the calculated ratio $\delta_{I\bar{a}c}/\delta_{II\bar{a}c}$ can only vary between $-0.07$ and $-0.8$ with the limits set by the F-position uncertainties. The nonoverlapping of these two regions makes it clear that tensor components $\epsilon_{I\bar{a}c}$ and $\epsilon_{II\bar{a}c}$ of the order of the diagonal $\bar{\epsilon}_i^+$ components necessarily have to be present. If, say $\epsilon_{I\bar{a}c}\simeq\epsilon_{II\bar{a}c}\simeq-7$ g/cm$^3$, the calculated $\sigma_{I\bar{a}c}/\sigma_{II\bar{a}c}$ can vary between $-1$ and $-4$, overlapping the spread in the experimental ratio ($-3.5$ to $-6.5$).

It is probably safe to state that $\sigma_{I\bar{a}c}<0$ and

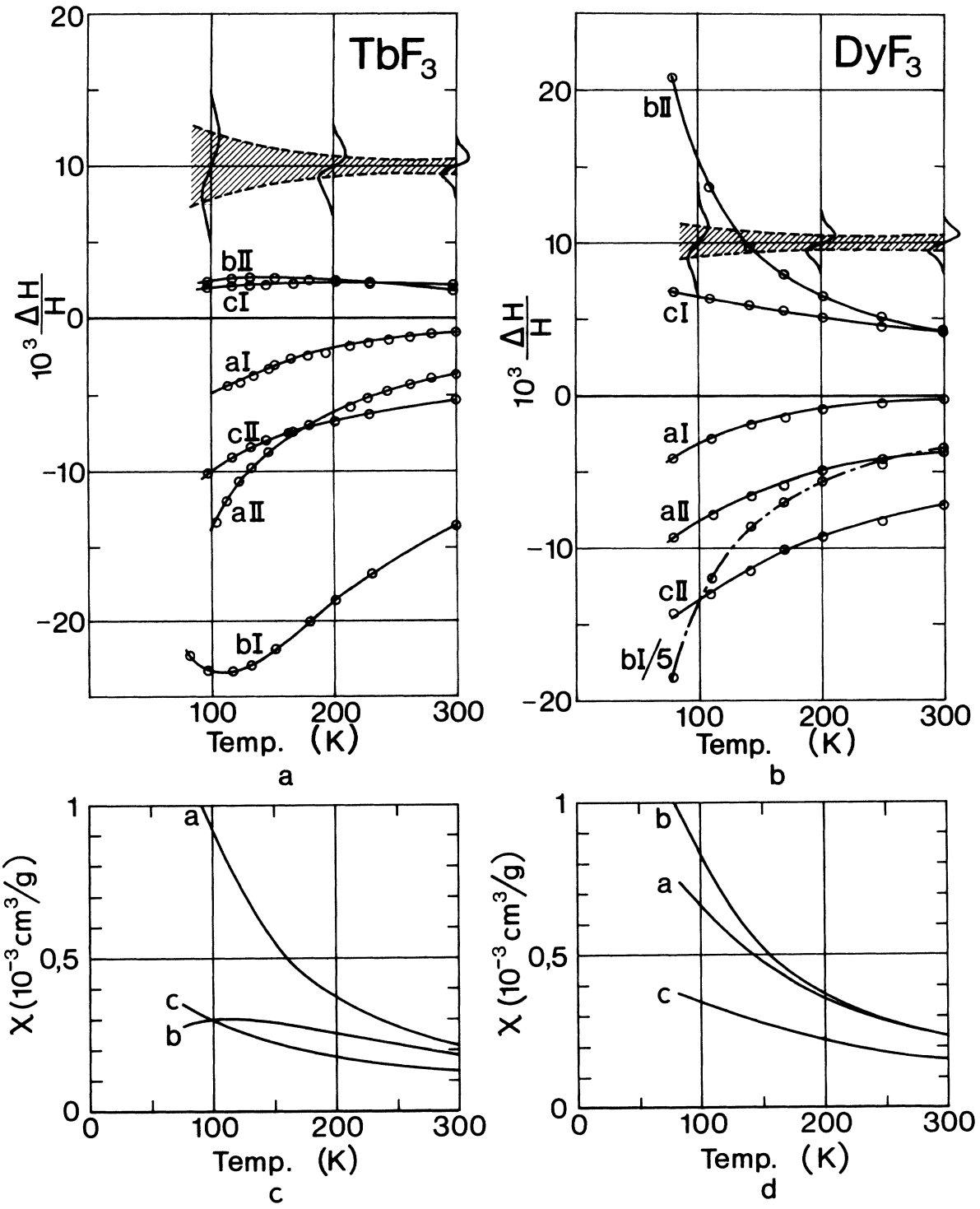


FIG. 4. Measured shifts $K_{\parallel}^{\alpha}(T)$ and $K_{\perp}^{\alpha}(T)$ with the applied field $\vec{H}_a$ parallel to $\alpha =$ the $a$, $b$, and $c$ axis. The linewidth (the peak to peak width of the NMR line derivative) vs temperature is also included. (a) $TbF_3$; (b) $DyF_3$ [note that $K_{\parallel}^{b}(T)$ values have been divided by 5]; for comparison the macroscopic susceptibilities for the two materials $\chi_a$, $\chi_b$, and $\chi_c$ are reproduced. (c) $TbF_3$; (d) $DyF_3$.

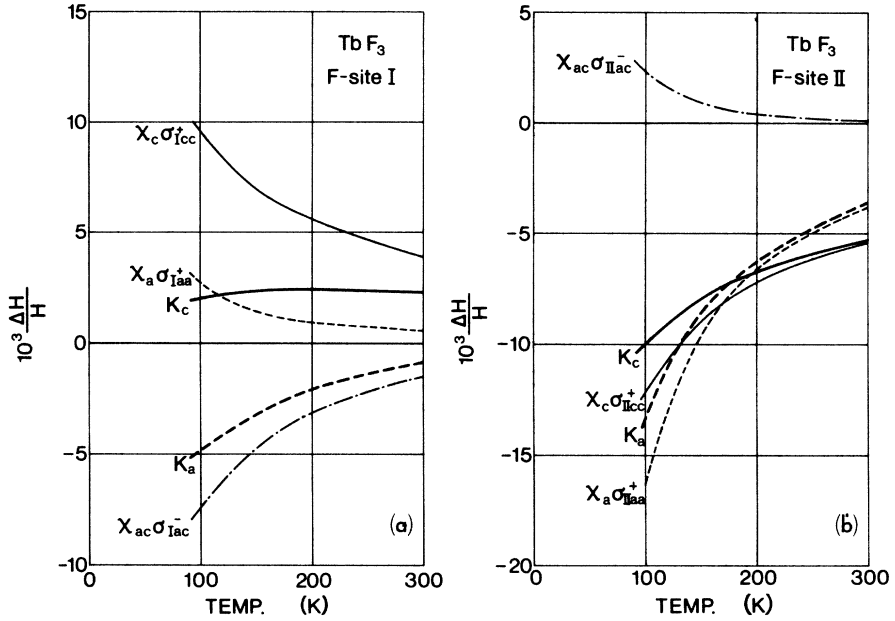


FIG. 5. Contributions to $K_i^a(T)$ and $K_i^c(T)$ for $TbF_3$. $K_i^a = \chi_a \sigma_{iaa}^+ + \chi_{ac} \sigma_{iac}^-$, $K_i^c = \chi_c \sigma_{icc}^+ + \chi_{ac} \sigma_{iac}^-$. (a) Site-I F; (b) Site-II F.

$\sigma_{IIac}^- > 0$. The opposite sign combination would require $|\epsilon_{IIac}^-| > 12$ g/cm$^3$, which seems to be an unreasonably large value compared to the values of the $\bar{\epsilon}_i^+$ components of Table IV. The fact that the sign of $\sigma_{iac}^-$ is known, connects the direction of the principal axes of the sublattice susceptibility tensors $\bar{\bar{\chi}}^A$ and $\bar{\bar{\chi}}^B$ in the $b$ plane to the surrounding structure. [If, furthermore, these directions do not change drastically (i.e., of the order of 45°) going down to liquid-He temperatures, also the $R$-moment tilt angles $\pm\theta$ in the zero field-ordered phase of $TbF_3$ are assigned to the two magnetically inequivalent parts of the unit cell. This assignment is not possible from the macroscopic magnetization measurements.] The orientation in the $b$ plane of the sublattice susceptibility easy axis $x$ (or of the $R$ moments in the ordered phase of $TbF_3$) is such that a vector from the nearest $F_{(I)}$ to the $R$ points between the $a$ axis and the $x$ axis (or the $R$ moment). The assignment is shown in Fig. 1.

If the $\sigma_{iac}^-$'s are in the neighborhood of the most likely values $\sigma_{Iac}^- \simeq -16$ g/cm$^3$ and $\sigma_{IIac}^- \simeq 4$ g/cm$^3$, the sublattice susceptibility angle $\theta(T)$ is ~29° and ~33° at 105 K for $TbF_3$ and $DyF_3$, respectively, whereas it increases to ~33° and ~35°, respectively,

TABLE V. Results compiled from Eqs. (5) and (9).

| Material | Site $i$ | Temperature (K) | 105 | 120 | 145 | 175 | 220 | 300 | $\delta_{iac}^-$[c] | $\Delta\delta_{iac}^-$[c] |
|---|---|---|---|---|---|---|---|---|---|---|
| $TbF_3$ | I | $\sigma_{Iac}^- \chi_{ac}$[a] | −7.17 | −6.25 | −4.83 | −3.72 | −2.65 | −1.60 | | |
| | | $\frac{1}{2}\sigma_{Iac}^- \tan 2\theta$[b] | −13 | −13 | −14 | −15 | −17 | −18 | −5 | ±4 |
| | II | $\sigma_{IIac}^- \chi_{ac}$[a] | 2.10 | 1.52 | 0.91 | 0.54 | (0.20) | (0.09) | | |
| | | $\frac{1}{2}\sigma_{IIac}^- \tan 2\theta$[b] | 3.4 | 3.2 | 2.8 | 2.2 | · · · | · · · | 13 | ±2 |
| $DyF_3$ | I | $\sigma_{Iac}^- \chi_{ac}$[a] | −5.70 | −4.88 | −3.86 | −3.10 | −2.27 | −1.61 | | |
| | | $\frac{1}{2}\sigma_{Iac}^- \tan 2\theta$[b] | −20 | −20 | −20 | −20 | −21 | −22 | −6 | ±4 |
| | II | $\sigma_{IIac}^- \chi_{ac}$[a] | 1.50 | 1.03 | 0.58 | (0.38) | (0.13) | (−0.03) | | |
| | | $\frac{1}{2}\sigma_{IIac}^- \tan 2\theta$[b] | 5.2 | 4.2 | 3.0 | · · · | · · · | · · · | 14 | ±2 |

[a]Experimental $\sigma_{iac}^- \chi_{ac}$ in units of $10^{-3}$. Accuracy $\sim \pm 0.3 \times 10^{-3}$.

[b]Calculated $\frac{1}{2}\sigma_{iac}^- \tan 2\theta = \sigma_{iac}^- \chi_{ac}/(\chi_a - \chi_c)$ in g/cm$^3$. Accuracy $\sim \pm 1.5$ g/cm$^3$. If $\sigma_{iac}^-$ is considered temperature independent, $\sigma_{Iac}^-/\sigma_{IIac}^-$ is $\sim -5 \pm 1.5$ for both $TbF_3$ and $DyF_3$.

[c]Calculated $\delta_{iac}^-$ and their uncertainty $\Delta\delta_{iac}^-$ (units of g/cm$^3$) due to the uncertainty in the F positions.

at 300 K. These statements concerning the absolute value and the temperature dependence of $\theta$ are of course very uncertain and should only be taken as an indication that the directions of the sublattice susceptibility principal axes do indeed stay nearly fixed from liquid-He temperatures to room temperatures. Fixed $b$-plane principal axes are in general not obvious, if this is not symmetry required. The axes are only fixed in the high-temperature limit, where $\overleftrightarrow{\chi}^A$ is entirely determined by the $R$ ion and the second-order terms of the crystal-field expansion at the $R$ of type $A$. The principal axes will point along the axes of that coordinate system, in which the second-order terms can be expressed solely by a linear combination of $O_2^0(\vec{J})$ and $O_2^2(\vec{J})$.

The fact that the principal axes seem to stay rather fixed far below the high-temperature limit is similar to what we have observed concerning the principal axes of the magnetization anisotropy in the basal plane of Li$R$F$_4$. They are not fixed by symmetry either, and yet their directions do not change appreciably from 1.3 to 150 K (Ref. 18).

## VII. CONCLUSIONS

The isotropic and anisotropic field shifts at the two chemically inequivalent F-ion sites in $TbF_3$ and $DyF_3$ have been found from $^{19}F$ NMR measurements in the temperature range 100–300 K.

The anisotropic field shifts are mainly due to the magnetic dipole fields. The anisotropic transferred hyperfine interactions are an order of magnitude less than the magnetic dipole interactions and probably roughly equal for the two materials. The isotropic field shifts, due to the isotropic transferred hyperfine interactions, are found to be negative and almost temperature independent and with nearly equal strength for both sites and both materials.

The sublattice susceptibility component $\chi_{ac}(T)$ is found to be comparable in size to the diagonal components, in the sense that it is not possible to interpret the measurements neglecting $\chi_{ac}(T)$. This is opposite to the findings for $TbF_3$ and $ErF_3$ by Mustafa *et al.*[8] The orientations of the principal axes of the two sublattices are assigned to definite $R$'s in the unit cell, i.e., to the crystalline surroundings of the $R$'s. This is not possible to do from the macroscopic magnetic measurements. Finally the temperature variations of the orientations of the sublattice susceptibility axes are found to be moderate.

It has turned out that even with great experimental care, it is hard to obtain an accurate determination of all transferred hyperfine parameters in crystal systems as complex as $RF_3$. This is due to (i) uncertainties in the exact positions of the fluorines, and (ii) the occurrence of magnetic sublattices, the principal axes directions of which are not known from other studies and furthermore may vary with temperature. Studies aiming at very accurate and reliable transferred hyperfine data should therefore preferably be done on crystals of simple structure with F and $R$ positions as well as susceptibility tensors axes completely fixed by symmetry. Some of these requirements are fulfilled by the Li$R$F$_4$ system on which we will report in the near future.

## ACKNOWLEDGMENTS

The authors are very grateful to Professor V. Frank for his continued interest and especially for helpful suggestions towards the interpretation of the present measurements. It is a pleasure to thank Dr. T. Johansson for the permission to use his unpublished susceptibility measurements for $DyF_3$. The unpublished report of NMR work on $TbF_3$ and $HoF_3$ by A. Reuveni and B. R. McGarvey is appreciated. One of us (P.E.H.) acknowledges his scholarship from the Danish Natural Science Research Council, Grant No. 511-7016. This work was partly supported by the Danish Natural Science Research Council Grant Nos. 511-3575 and 511-7016.

*Present address: Danfoss A/S, 6430 Nordborg Als, Denmark.

[1]E. A. Baturina, Y. A. Luk'Yanychev, and O. T. Malyuchkov, Sov. Phys.-Solid State 7, 1527 (1965).

[2]S. P. Gatuda, A. G. Lundin, Y. V. Gagarinskii, L. R. Balsanova, and L. A. Khripin, Sov. Phys.-JETP 24, 469 (1967).

[3]V. Saraswati and R. Vijayaraghavan, Phys. Lett. 21, 363 (1968).

[4]S. L. Carr and W. G. Moulton, J. Magn. Reson. 4, 400 (1971).

[5]S. K. Malik, R. Vijayaraghavan, and P. Bernier, J. Magn. Reson. 4, 400 (1971).

[6]A. G. Lundin and S. P. Gabuda, Bull. Acad. Sci. USSR 1, 90 (1968).

[7]S. A. Al'tshuler, F. L. Aukhadeev, I. I. Valeev, I. S. Konov, B. Z. Malkin, and M. A. Teplov, JETP Lett. 16, 164 (1972).

[8]M. R. Mustafa, B. R. McGarvey, and E. Banks, J. Magn. Reson. 25, 341 (1977): A Reuveni and B. R. McGarvey, J. Magn. Reson. (unpublished).

[9]A. Zalkin and D. H. Templeton, J. Am. Chem. Soc. 75, 2453 (1953).

[10]L. Holmes and H. J. Guggenheim, J. Phys. (Paris) 32, C1-501 (1971).

[11]T. Johansson (unpublished data).

[12]P. E. Hansen, T. Johansson, and R. Nevald, Phys. Rev. B 12, 5315 (1975).

[13]P. E. Hansen and R. Nevald, Phys. Rev. B 16, 146 (1977).
[14]H. J. Guggenheim, J. Appl. Phys. 34, 2482 (1963).
[15]M. R. Mustafa, W. E. Jones, B. R. McGarvey, M. Greenblatt, and E. Banks, J. Chem. Phys. 62, 2700 (1975).
[16]B. R. McGarvey, J. Chem. Phys. 65, 962 (1976).
[17]R. Nevald and P. E. Hansen (unpublished data).
[18]R. Nevald and P. E. Hansen, Physica (Utr.) B 86–88, 1445 (1977).